Chinese Chemical Letters 33 (2022) 5162–5168

Contents lists available at ScienceDirect

Chinese Chemical Letters

journal homepage: www.elsevier.com/locate/cclet

Boosting the photocatalytic nitrogen reduction to ammonia through adsorption-plasmonic synergistic effects

Yunni Liu[b], Xingyu Ye[a], Ruping Li[a], Ying Tao[b], Chi Zhang[b], Zichao Lian[c], Dieqing Zhang[a,*], Guisheng Li[a,b,c,*]

[a] The Education Ministry Key Lab of Resource Chemistry, Shanghai Key Laboratory of Rare Earth Functional Materials, College of Chemistry and Materials Science, Shanghai Normal University, Shanghai 200234, China
[b] School of Environmental and Geographical Sciences, Shanghai Normal University, Shanghai 200234, China
[c] School of Materials Science and Engineering, University of Shanghai for Science and Technology, Shanghai 200093, China

ARTICLE INFO

Article history:
Received 28 October 2021
Revised 1 December 2021
Accepted 28 January 2022
Available online 3 February 2022

Keywords:
Photocatalysis
Plasmon
Au
MIL-100(Cr)
Nitrogen fixation

ABSTRACT

Ammonia is one of the most essential chemicals in the modern society but its production still heavily relies on energy-consuming Haber-Bosch processes. The photocatalytic reduction of nitrogen with water for ammonia production has attracted much attention recently due to its synthesis under mild conditions at room temperature and atmospheric pressure using sunlight. Herein, we report a high-performance Au/MIL-100(Cr) photocatalyst, comprising MIL-100(Cr) and Au nanoparticles in photocatalytic nitrogen reduction to ammonia at ambient conditions under visible light irradiation. The optimized photocatalyst (*i.e.*, 0.10Au/MIL-100(Cr)) achieved the excellent ammonia production rate with 39.9 μg g_{cat}^{-1} h^{-1} compared with pure MIL-100(Cr) (2.73 μg g_{cat}^{-1} h^{-1}), which was nearly 15 times that on pure MIL-100(Cr). The remarkable activity could be attributed to the adsorption-plasmonic synergistic effects in which the MIL-100(Cr) and Au are responsible to the strong trapping and adsorption of N_2 molecules and photo-induced plasmonic hot electrons activating and decomposing the N_2 molecules, respectively. This study might provide a new strategy for designing an efficient plasmonic photocatalyst to improve the photocatalytic performance of N_2 fixation under visible light irradiation.

© 2022 Published by Elsevier B.V. on behalf of Chinese Chemical Society and Institute of Materia Medica, Chinese Academy of Medical Sciences.

Ammonia is a commodity chemical for human society in industry and agriculture, and also plays an important role as energy carrier for hydrogen [1–4]. The ever-increasing demand for ammonia has driven much research interests in the large scale of its production. In general, the organisms convert the atmospheric nitrogen to ammonia by the enzyme nitrogenase which is the main way to produce ammonia in nature [5,6]. Currently, most of its industrial production still depends on the traditional Haber-Bosch processes which require a harsh reaction condition (400-500 °C and 150-50 atm), resulting in the large energy consumption [7,8]. Due to the strong bond strength of N≡N (940.95 kJ/mol) for N_2 dissociation [1,9], it is still a great challenge for green synthesis ammonia from N_2 and H_2O under room temperature and ambient pressure [10,11]. Recently, the photocatalytic reduction of nitrogen utilizes the water as proton source as well as reaction solvent, and solar light as energy input, has been considered as a sustainable technology for the synthesis of ammonia [12–17]. It is urgent to develop highly efficient semiconductor catalysts to overcome the slow adsorption/activation kinetics of N_2 molecules. To date, among various photocatalysts, titania-based materials are one of the most researched photocatalysts owing to their excellent stability, environmentally friendly feature and low cost [18–22]. Furthermore, the modifications of metal oxides by heteroatoms doping, surface modification or the introduction of surface vacancies have been verified to enhance their photocatalytic performance at ambient conditions with light irradiation [20,23]. Taking TiO_2 as an example, incorporating Fe as a dopant in the TiO_2 nanoparticles can generate oxygen vacancies and dopant energy levels, and the further modification of F is conducive to the adsorption and activation of N_2 molecule. Therefore, F-Vo-TiO_2 and F-Fe:TiO_2 both exhibit a higher NH_3 production rate and faradaic efficiency (FE) than pristine TiO_2 [24,25].

Beyond that, the localized surface plasmon resonance (LSPR) is also a powerful way to improve the utilization of solar light for photocatalysts [20,21,26-28]. The hot electrons generated by LSPR can drive many chemical reactions, such as CO_2 reduction and wa-

* Corresponding authors.
E-mail addresses: dqzhang@shnu.edu.cn (D. Zhang), liguisheng@shnu.edu.cn (G. Li).

https://doi.org/10.1016/j.cclet.2022.01.076
1001-8417/© 2022 Published by Elsevier B.V. on behalf of Chinese Chemical Society and Institute of Materia Medica, Chinese Academy of Medical Sciences.

ter splitting by using plasmonic metal-based heterostructures [29–34]. In a typical chemical reaction, the reactants need enough energy to cross a threshold to complete the reaction. The previous reports have demonstrated that the hot electrons whose temperature can be as high as about 1100 °C generated on illuminated Au NPs will lose energy to the reactants, pushing them to cross that threshold, thereby speeding up the chemical reaction [35]. Thus the hot electrons also can dissociate and desorb both polar and non-polar molecules [36,37], which is also beneficial to enhance the performance of photocatalytic N_2 reduction reaction (NRR) [28,38,39].

The solubility of N_2 in water is very low (8.21×10^{-4} mol/L at 0 °C when the N_2 pressure above water is 0.790 atm), thus, increasing the concentration of N_2 on the surface of catalyst is also crucial to increase the kinetic processes of NRR. Metal-organic frameworks (MOFs), an emerging porous material with large surface area, have an excellent absorption ability for the gas such as N_2, CO_2, CH_4 [40–46]. Furthermore, unsaturated transition metal sites in MOFs, such as Cr, Mo and Bi, have been reported to possess the abilities of the adsorption and reduction of N_2 [47–51]. For example, at 283 K and 1 bar of nitrogen gas, MIL-100(Cr) has been proved to capture N_2 effectively (1.64 mmol/g), which outperform the benchmark zeolite LiX (1.27 mmol/g), because of the presence of unsaturated Cr(III) sites [52–54].

In this work, we combine the LSPR effect of Au NPs and the strong N_2-adsorption ability of MIL-100(Cr) together for constructing an effective visible-light driving photocatalyst for NRR under ambient conditions. The as-obtained adsorption-plasmonic synergistic photocatalyst Au/MIL-100(Cr) exhibited an obvious enhancement about 18.4 times higher for ammonia formation compared to that of the pure MIL-100(Cr) under visible-light irradiation. A highest apparent quantum efficiency (AQE) (0.07%) was achieved for reducing N_2 to ammonia under the visible-light irradiation ($\lambda = 550$ nm). The superior activity could be ascribed to the hot-electron-induced N_2 dissociation and reduction to ammonia on the surface of the illuminated Au NPs and the strong N_2 absorption ability of MIL-100(Cr). This work provides a promising strategy for the design of photocatalysts with the effective adsorption-plasmonic synergistic effect for artificial N_2 fixation.

The preparation procedures of Au/MIL-100(Cr) catalyst were schematically presented in Fig. 1a. The MIL-100(Cr) was firstly prepared *via* hydrothermal method using metallic chromium and trimesic acid as precursors and the Au nanoparticles (Au NPs) were deposited on MIL-100(Cr) using $HAuCl_4$ as the precursor and trisodium citrate as reducing and stabilizing agent. The morphologies of the as-synthesized MIL-100(Cr) and 0.10Au/MIL-100(Cr) were investigated by FESEM and TEM (Figs. 1b-d). The as-synthesized MIL-100(Cr) exhibited irregular blocky structure (Figs. 1b and c). Au NPs were successfully deposited on the surface of MIL-100(Cr) with particle sizes ranging from 20 nm to 30 nm, and the overall structure of MIL-100(Cr) was not damaged after the deposition of Au NPs (Fig. 1d and Fig. S1 in Supporting information). Fig. 1e shows the XRD patterns of the as-synthesized MIL-100(Cr) and 0.10Au/MIL-100(Cr). All diffraction peaks of as-prepared MIL-100(Cr) matched well to the previously reported patterns [53,55], indicating the successful synthesis of MIL-100(Cr). After the Au deposition, the significant characteristic peaks located at 38.2°, 44.4°, 64.6°, 77.5°, corresponding to the (111), (200), (220), (311) crystal planes of Au (JCPDS No. 04-0784), respectively. This result indicated that the standard face-centered cubic (fcc) Au nanoparticles were formed on the surface of MIL-100(Cr). Besides, the diffraction peaks associated to MIL-100(Cr) were still observed in 0.10Au/MIL-100(Cr) indicating the reservation of the MIL-100(Cr) structure. In addition, no obvious differences of the peaks contributed by the functional groups of MIL-100(Cr) of MIL-100(Cr) and 0.10Au/MIL-100(Cr) in the FT-IR spectra (Fig. S2 in Supporting information). As the TPD experiments revealed, both MIL-100(Cr) and 0.10Au/MIL-100(Cr) catalysts exhibited physical adsorption (175 °C) and chemical adsorption (300 °C) of N_2, among which the characteristic peaks of 0.10Au/MIL-100(Cr) were higher, indicating 0.10Au/MIL-100(Cr) had a stronger adsorption capacity for N_2 (Fig. S3a in Supporting information). Particularly, the chemical environment of the metal center (Cr) of the MIL-100(Cr) was well maintained after the deposition of Au NPs, leading to the strong N_2 adsorption capability of the as-formed 0.10Au/MIL-100(Cr) catalyst. The results indicated that the excellent N_2 adsorption capacity of 0.10Au/MIL-100(Cr) was beneficial to the activation and reduction of N_2 due to the thermal electrons generated by Au nanoparticles. The BET surface areas of MIL-100(Cr) and 0.10Au/MIL-100(Cr) were determined to be 1304 and 999 m^2/g, respectively (Fig. 1f). In addition, the pore size distribution curves showed that the catalyst changed from mesoporous structure (4-5 nm) to microporous structure (<2 nm) after loading Au NPs (Fig. S3b in Supporting information). Therefore, we believe that the decreased surface area of 0.10Au/MIL-100(Cr) catalyst may be attributed to the presence of Au NPs, which block some pores of the MIL-100(Cr).

The as-obtained MIL-100(Cr) and 0.10Au/MIL-100(Cr) were further characterized by the XPS measurements. Fig. 2a shows the XPS spectra of MIL-100(Cr) and 0.10Au/MIL-100(Cr) and a typical Au peak was observed in Au/MIL sample. In addition, the Cr, O and C elements coming from MIL-100(Cr) were also observed in the as-obtained Au/MIL sample. The high-resolution Au 4f XPS spectrum of Au/MIL (Fig. 2b) revealed two peaks located at 87.9 eV and 84.3 eV, which were assigned to Au $4f_{5/2}$ and $4f_{7/2}$ of metallic Au, indicating the complete reduction of $AuCl_4^-$ to metallic Au. Fig. 2c displays the high-resolution Cr 2p XPS spectra of MIL-100(Cr) and 0.10Au/MIL-100(Cr). The characteristic peaks at 586.9 eV and 577.4 eV can be assigned to Cr $2p_{1/2}$ and Cr $2p_{3/2}$ of Cr (III) species. According to previous literatures, the unsaturated Cr (III) sites enabled MIL-100(Cr) to selectively capture N_2 molecules [54]. And a slight shift towards the lower binding energy of Cr 2p in 0.10Au/MIL-100(Cr) sample compared to that of MIL-100(Cr) states was observed. Such results indicated that the 0.10Au/MIL-100(Cr) photocatalyst could selectively adsorb N_2 molecules with the assistant of Cr(III) sites in MIL-100(Cr) and the unsaturated Cr (III) sites obtained the hot electrons generated by LSPR effect of Au NPs. The UV-vis diffuse reflectance spectra (UV-vis DRS) was utilized to illustrate the light absorption range and LSPR effect of the samples. As shown in Fig. 2d, the UV-vis DRS spectrum of MIL-100(Cr) exhibited two obvious adsorption peaks at 440 nm and 600 nm in visible light sections which can be identified to d-d transitions $A_{2g} \rightarrow g_{1g}$ and $A_{2g} \rightarrow g_{2g}$ of Cr(III) in MIL-100(Cr) [56]. The UV-vis DRS spectra also confirmed that the Au NPs have been successfully deposited on the MIL-100(Cr). With the introduction of Au NPs on MIL-100(Cr), the adsorption intensity increased in visible-light regions, and the as-synthesized 0.10Au/MIL-100(Cr) also displays an apparent adsorption band at 538 nm which can be attributed to LSPR excitation of Au NPs.

The activity of MIL-100(Cr) and 0.10Au/MIL-100(Cr) for photocatalytic NRR to ammonia were evaluated by using water as the proton source and solvent under ambient conditions with the irradiation of visible light ($\lambda > 420$ nm). The photocatalytic NRR performance with different contents of Au NPs was investigated to give the optimal Au NPs amount. Fig. S4a (Supporting information) showed the XRD patterns of catalysts with different Au loadings, showing that the intensity of Au diffraction peaks increased with the increase of Au loading. The BET data (Fig. S4b in Supporting information) showed that as the Au loading increased, the specific surface area of the catalyst decreased. The reason was that the Au loading blocked part of the pores on the MIL-100(Cr) surface. As revealed in Fig. 3a, the ammonia formation rate was firstly greatly enhanced upon increasing the amount of Au NPs from around 5%

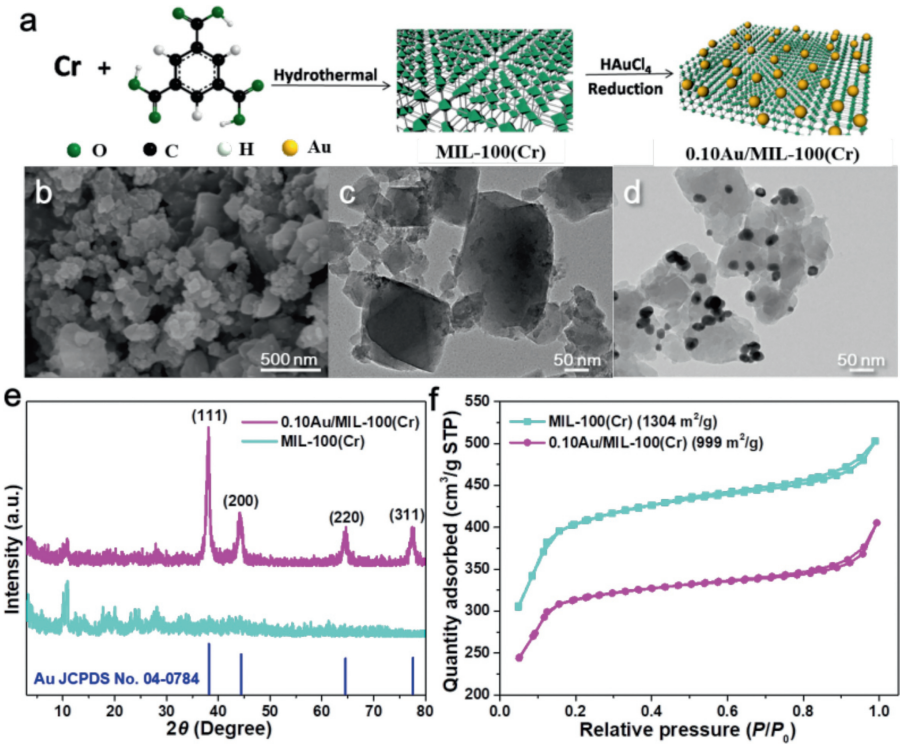

Fig. 1. (a) The schematic illustration of the preparation of Au/MIL-100(Cr). (b) The representative SEM and (c) TEM images of MIL-100(Cr). (d) TEM image of 0.10Au/MIL-100(Cr), (e) XRD patterns and (f) the nitrogen adsorption/desorption isotherms curves of MIL-100(Cr) and 0.10Au/MIL-100(Cr).

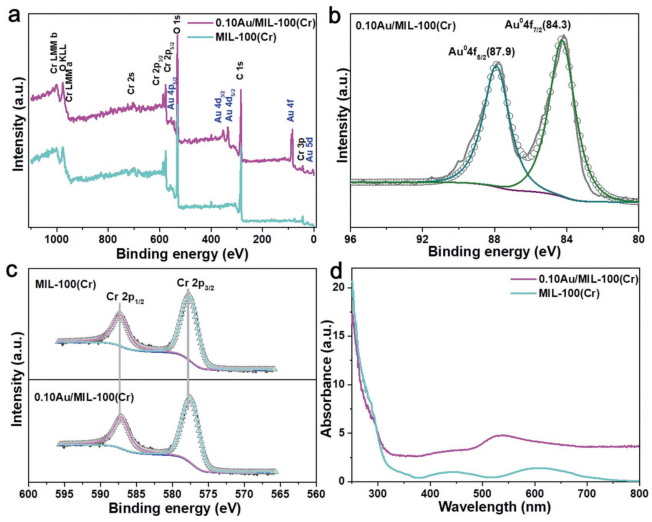

Fig. 2. (a) XPS spectra of MIL-100(Cr) and 0.10Au/MIL-100(Cr); (b) high-resolution Au 4f XPS spectrum of 0.10Au/MIL-100(Cr); (c) high-resolution Cr 2p spectra of MIL-100(Cr) and 0.10Au/MIL-100(Cr). (d) The UV-vis DRS spectra of MIL-100(Cr) and 0.10Au/MIL-100(Cr).

to 10%, owing to the more active sites and more hot electrons generated by LSPR effect. 0.10 Au/MIL-100(Cr) achieved the highest ammonia production rate at 39.9 μg g_{cat}^{-1} h^{-1}. In addition, the continued increment of Au contents led to the decrease of ammonia formation rate, which may be contributed to the decrease of surface areas with lower N_2 adsorption capacities. These results suggest that the balance between the amount of active sites and trapped N_2 molecules on the surface of Au/MIL-100(Cr) is crucial for the reduction of N_2 to produce NH_3.

As shown in Fig. 3b, an obvious amount of ammonia was observed after 12 h using 0.10Au/MIL-100(Cr) as photocatalysts, and its amount was increased linearly along with the reaction time. As a comparison, the ammonia formation rate is very low on MIL-100(Cr) under the same conditions. The ammonia formation rate on 0.10Au/MIL-100(Cr) catalyst surface reached 39.93 μg g_{cat}^{-1} h^{-1} which is about 15 times higher than that on pure MIL-100(Cr) surface [57–60]. Such difference indicates that N_2 molecules can be effectively dissociated to form ammonia on the surface of Au NPs due to the activation of plasmonic hot electrons. Control experiments were also performed to confirm the source of nitrogen element in ammonia. When the N_2 was replaced by argon in the reaction system (Fig. 3b), no ammonia was detected under the same conditions indicating the nitrogen atoms in ammonia are originated from the N_2. This photocatalytic NRR process was also conducted in dark conditions for both MIL-100(Cr) and 0.10Au/MIL-100(Cr) catalysts. However, no ammonia was observed (Fig. S5 in Supporting information). That illustrated that the light irradiation provides the required energy input for this photocatalytic NRR process. To identify the role of water during the photocatalytic NRR process, water was replaced by acetonitrile (CH_3CN) as aprotic solvent and, as shown in Fig. 3c, no ammonia was generated indicating water is the proton source in this process. To further illustrate the activity of 0.10Au/MIL-100(Cr) for photocatalytic NRR process, various control experiments were performed and the ammonia formation rates were shown in Fig. 3d. Upon introducing the electron scavenger ($AgNO_3$) to consume the hot-electrons generated by Au, the ammonia evolution rate was greatly suppressed. The ammonia evolution rate was greatly suppressed with the addition of the electron scavenger ($AgNO_3$) indicating the hot-electrons generated by Au are the key driving force to reduce N_2 into ammonia. In addition, the hole scavenger, methanol, was also added into this system and the ammonia formation rate was obviously promoted on 0.10Au/MIL-100(Cr) surface. This demonstrated that the rapid consumption of holes was favorable for the photocatalytic NRR process for ammonia production. In the absence of hole scavenger, the holes will be consumed by the H_2O *via* oxidizing OH^- to O_2 and

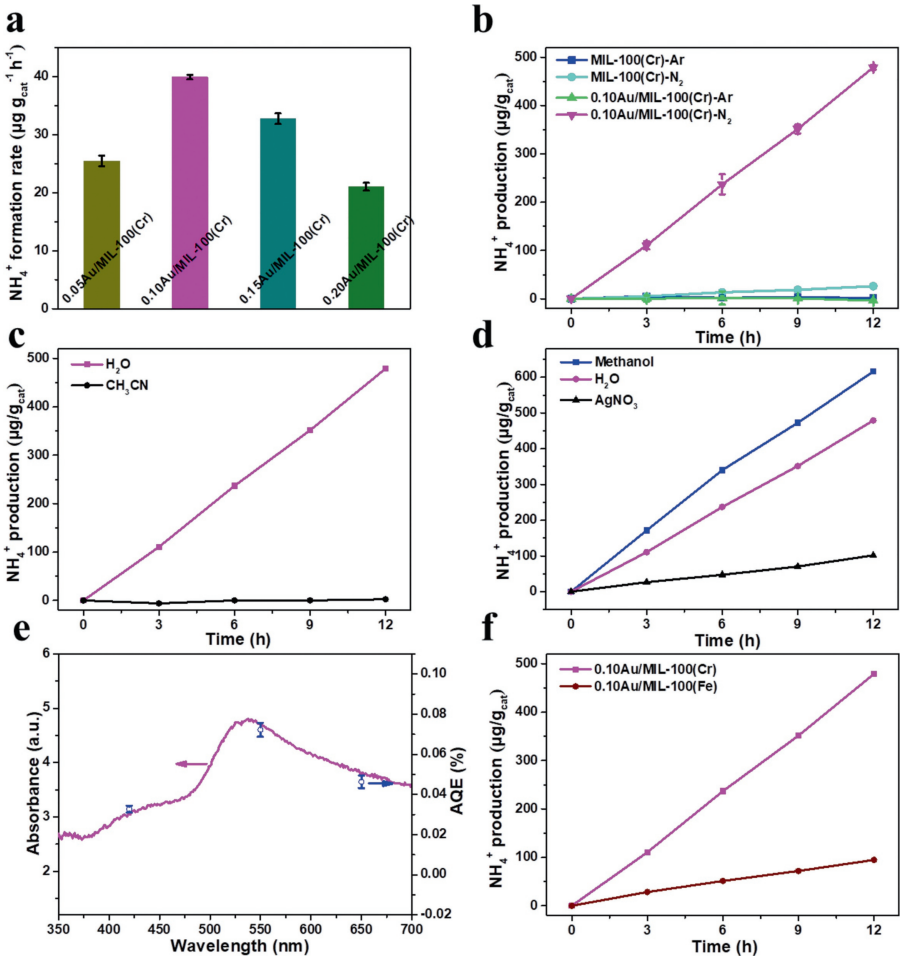

Fig. 3. (a) NH_4^+ formation rate of catalysts with different loading of Au under visible light (>420 nm); (b) NH_4^+ formation rate of catalysts under visible light (>420 nm); (c) control experiments of photocatalytic N_2 fixation with using aprotic solvent (CH_3CN); (d) photocatalytic NRR performance with 0.10Au/MIL-100(Cr) using $AgNO_3$ as the electron scavenger and methanol as the hole scavenger; (e) wavelength-dependent apparent quantum efficiency of the as-prepared 0.10Au/MIL-100(Cr) under monochromatic light irradiation, in reference to its UV-vis diffuse reflectance spectra; (f) the NH_4^+ production of catalysts with different ligand centers.

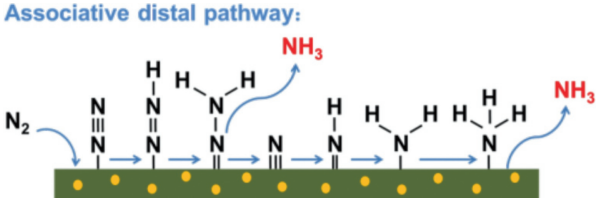

Fig. 4. Possible reaction mechanisms for the photocatalytic N_2 fixation to form NH_3.

O_2 was indeed observed in this process (Fig. S6a in Supporting information). That means water was oxidized by the holes with the formation of O_2, and the generated protons (H^+) would be utilized for driving the ammonia production. Besides, although the byproducts, NO_3^-, was also tracked, its yield can be neglected compared to the ammonia formation rate during the process of photocatalytic N_2 fixation (Fig. S6b in Supporting information). Accordingly, the overall reaction of the photocatalytic N_2 fixation in the proposed reaction system could be described as the following equation:

$$2N_{2(g)} + 6H_2O_{(l)} \rightarrow 4NH_{3(g)} + 3O_{2(g)} \quad (1)$$

To further investigate the LSPR effect of Au NPs and obtain the action spectrum for photocatalytic NRR process, the activity tests of light wavelength-dependence for ammonia production were measured in absence of scavenger with the irradiation of different LED monochromatic light under the ambient conditions. As shown in Fig. 3e, 0.10Au/MIL-100(Cr) can be utilized to drive the ammonia evolution under light irradiation with different monochromatic wavelengths. It was interesting that the highest value (0.07%) of apparent quantum efficiency (AQE) for NRR was obtained under 550 nm light irradiation. The AQE values would be greatly decreased by choosing shorter (420 nm) or longer (650 nm) wavelength. Therefore, the results could be concluded that the photocatalytic NRR process was mainly induced by the visible-light induced LSPR effect on Au NPs. The as-formed 0.10Au/MIL-100(Cr) framework could be utilized as an efficient and energy-saving photocatalyst for the reduction of nitrogen under visible and near IR light irradiation.

The unsaturated Cr(III) that existed in MIL-100(Cr) has been reported as effective sites for the adsorption of N_2 at ambient conditions due to its strong binding interaction with N_2 [54]. As well known, in nature, plants use nitrogenase to fix nitrogen, in which Fe is the active center. On the other hand, as for the N_2 adsorption isotherms, MIL-100(Fe) had been confirmed that it was inferior to MIL-100(Cr) [54]. Thus, in order to verify the role of unsaturated Cr(III) sites for its N_2 adsorbed ability during the photocatalytic NRR process, a similar MOFs, MIL-100(Fe) was prepared by replacing the Cr ligand center into Fe as the support for Au NPs. The SEM images of MIL(Fe) (Fig. S7a in Supporting information) and 0.10Au/MIL-100(Fe) (Fig. S7b in Supporting information) also showed no structure changes after Au deposition. The

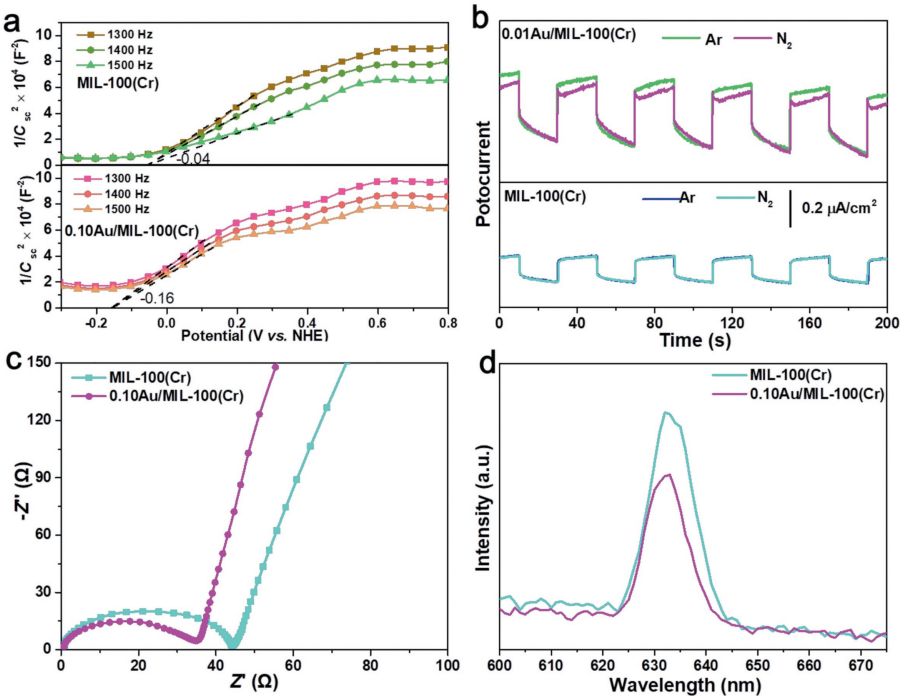

Fig. 5. (a) The Mot-Schottky plots of MIL-100(Cr) and 0.10Au/MIL-100(Cr). (b) Transient photocurrent responses of MIL-100(Cr) and 0.10Au/MIL-100(Cr) under different gas conditions. (c) Electrochemical impedance spectroscopy (EIS) of MIL-100(Cr) and 0.10Au/MIL-100(Cr). (d) Photoluminescence (PL) spectra of MIL-100(Cr) and 0.10Au/MIL-100(Cr).

XRD pattern of 0.10Au/MIL-100(Fe) (Fig. S8a in Supporting information) also showed the typical diffraction peaks from the face-centered cubic (fcc) Au nanoparticles. Meanwhile, the FT-IR spectrum (Fig. S8b in Supporting information) of 0.10Au/MIL-100 (Fe) was the same as that of the pure MIL-100(Fe), suggesting that the functional groups of MIL-100(Fe) were well maintained after the deposition of Au NPs. The Au content (Table S2 in Supporting information) in 0.10Au/MIL-100(Fe) sample was 11.03% which was much closed to that in the composite of 0.10Au/MIL-100(Cr). As shown in Fig. 3f, the NH_4^+ formation rate on Au/MIL-100(Fe) is 94.81 μg/g_{cat} which is only 19.8% of that for the 0.10Au/MIL-100(Cr) sample (479.1 μg/g_{cat}) after 12 h under the same conditions and such significantly decreased NH_4^+ formation rate proves the N_2 capture and adsorption by the unsaturated Cr(III) sites in MIL-100(Cr) is crucial for NRR. It was noted that no N_2H_4 evolution was observed in the process of photocatalytic NRR as shown in Fig. S9 (Supporting information). These results indicated that the as-formed 0.10Au/MIL-100(Cr) could present an associative distal hydrogenation pathway for photocatalytic NRR [47,50]. During the NRR process, the first step in this NRR pathway was N_2 dissociative, then the *N species coupled with one proton step by step to form $*NH_3$ species, finally the $*NH_3$ species desorbed from the catalyst surface and formed ammonia ion in the solution (Fig. 4).

To further explore the mechanism, the photoelectrochemical measurements are performed. The Mott-Schottky plots are a general way to determine the charge carrier concentrations and the flat band potential (E_{fb}) of the catalysts and the E_{fb} value could be calculated from the intercept of the axis with potential values. The positive slope of the Mott-Schottky plots demonstrated the photocatalyst was the n-type character of the electronic band structure in which electrons as the majority charge carriers [61]. As shown in Fig. 5a, the E_{fb} value for the 0.10Au/MIL-100(Cr) was −0.16 V *vs.* NHE which is more negative than that −0.04 V *vs.* NHE on the pure MIL-100(Cr). For most of n-type semiconductor catalysts, the conduction band potential (E_{cb}) was approximately 0.1-0.2 V negative than the E_{fb} value [62]. Therefore, the E_{cb} value of

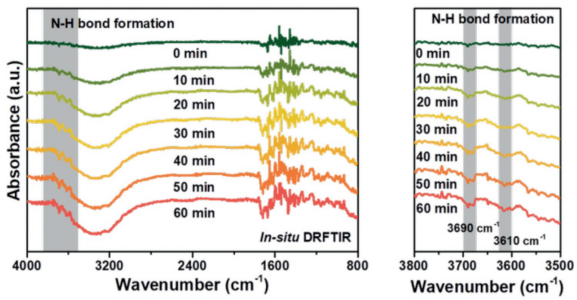

Fig. 6. *In-situ* DRFTIR spectra for N_2 reduction on the 0.10Au/MIL-100(Cr) surface following purging with N_2 and H_2O under LED light exposure ($\lambda = 420$ nm).

0.10Au/MIL-100(Cr) was calculated to be about −0.36 V *vs.* NHE. It was true that the reduction potential for directly reducing N_2 to $N_2^-{}_{(aq)}$ ($N_2 + e^- \rightarrow N_2^-{}_{(aq)}$) was −4.2 V *vs.* NHE, and the proton-coupled electron transfer reaction ($N_2 + H^+ + e^- \rightarrow N_2H$) exhibited a more accessible reduction potential of −3.2 V *vs.* NHE. It seems to be thermodynamically unfavorable for N_2 reduction because the E_{cb} of 0.10Au/MIL-100(Cr) was not negative enough to drive the N_2 fixation. Therefore, it could be inferred that the hot electrons generated on the surface of Au NPs are the driving factor to activate N_2 molecules and boost N_2 dissociation to produce ammonia, due to the LSPR effect on the surface of Au NPs.

To illustrate the interfacial electron transfer, the transient photocurrent responses on the pure MIL-100(Cr) and 0.10Au/MIL-100(Cr) were recorded under the visible light irradiation in both Ar and N_2 atmosphere. As shown in Fig. 5b, the photocurrent responses in Ar atmosphere are derived from the transfer of photogenerated electrons to electrode. The transient photocurrents decreased after pumping N_2 into the electrolyte for 30 min compared with that in Ar-saturated atmosphere under the same conditions. The decrease of the photocurrent could be ascribed to the competitive interfacial electron transfer to N_2 molecules which were

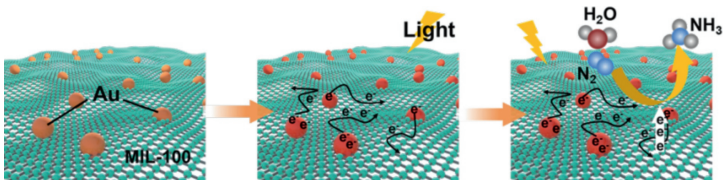

Fig. 7. Schematic illustration of the photocatalytic N_2 fixation over Au/MIL in which water serves as both the solvent and proton source.

adsorbed on the surface of Au/MIL-100(Cr). In comparison, in absence of LSPR effect, the photocurrent in N_2 atmosphere was almost the same as that in Ar atmosphere for the MIL-100(Cr). The difference between 0.10Au/MIL-100(Cr) and MIL-100(Cr) could be well explained by the indispensable role of LSPR which generates the hot electrons on the Au NPs for both the adsorption and activation of N_2.

In addition, electrochemical impedance spectroscopy (EIS) was used to evaluate the charge transfer resistance. As revealed in Fig. 5c, the resistant of the as-prepared 0.10Au/MIL-100(Cr) was smaller than that of the pure MIL-100(Cr), indicating a faster charge transfer rate in the presence of Au NPs. The photoluminescence (PL) spectra were also performed for clarifying the recombination rates of electron-hole pairs on 0.10Au/MIL-100(Cr) and MIL-100(Cr) surfaces. As displayed in Fig. 5d, the PL intensity of 0.10Au/MIL-100(Cr) possessed a weaker emission peak than that of MIL-100(Cr) at 632.5 nm, verifying that the Au NPs on MIL-100(Cr) could inhibit the recombination of photo-generated carrier which will make higher carrier separation efficiency for increasing the performance of photocatalytic NRR of 0.10Au/MIL-100(Cr) under ambient conditions.

To prove the formation of ammonia after the photoreaction, *in-situ* DRFTIR had been conducted. As shown in Fig. 6, the reference spectrum was collected at the beginning of the N_2 photo-reduction reaction with the reaction time of 0 min. After 10 minutes, two small peaks at ~3610 cm^{-1} and ~3690 cm^{-1} appeared, and these two peaks could be attributed to the vibration of N−H bond. When the photo-reduction reaction time increased, the intensities of these two vibration peaks also increased indicating the formation of N−H bonds on the surface of 0.10Au/MIL-100(Cr) were the intermediates for the N_2 reduction to NH_3.

Based on the above results, the photocatalytic NRR processes on 0.10Au/MIL-100(Cr) could be illustrated in Fig. 7. In the 0.10Au/MIL-100(Cr) composites, MIL-100(Cr) provides abundant sites for N_2 adsorption on the surface of 0.10Au/MIL-100(Cr) [52–54]. Meanwhile, the LSPR effect of Au NPs would facilitate the dissociation processes of N_2 molecules by the generation of hot electrons [21,60,63]. When the reaction occurs, the hot electrons are injected into the antibonding orbital of N_2 on the surface of MIL-100(Cr), and thus the N≡N bonds would be broken for the evolution of ammonia in the electron-proton couple process. Therefore, the synergistic effect between the Au NPs and MIL-100(Cr) allowed an effectively photocatalytic NRR process by using N_2 and water as precursors under visible-light irradiation.

The stability of the 0.10Au/MIL-100(Cr) for N_2 fixation process was also studied by cycling photocatalytic reactions. As shown in Fig. S10 (Supporting information), no obvious decrease in activity was observed after five cycles, illustrating the excellent photocatalytic stability of 0.10Au/MIL-100(Cr) during the N_2 fixation reactions under visible-light irradiation. In addition, various characterizations of the as-formed 0.10Au/MIL-100(Cr) after being used for five times were also performed to investigate its structural stability. The XRD pattern of the recycled samples suggested that 0.10Au/MIL-100(Cr) could be well maintained after the photocatalytic NRR reactions (Fig. S11a in Supporting information). The FT-IR spectra showed that the functional groups of 0.10Au/MIL-100(Cr) were also in accordance with the fresh photocatalyst (Fig. S11b in Supporting information).

In summary, we demonstrated that N_2 can be efficiently reduced to ammonia in absence of any scavenges by using 0.10Au/MIL-100(Cr) as photocatalyst at room temperature and atmospheric pressure with visible light irradiation. The hot electrons generated by LSPR effect of Au NPs activate N_2 molecules and drive its dissociation to form ammonia by injecting hot electrons into MIL-100(Cr) to break the bonds of N_2 molecules. Such Au/MIL series catalysts exhibited significantly increased activity and high selectivity to ammonia production in photocatalytic NRR process compared to that of the pure MIL-100(Cr) frameworks. The ammonia formation rate on Au/MIL catalyst reached to 39.93 μg g_{cat}^{-1} h^{-1}, about 14.5 times higher than that on the pure MIL-100(Cr) (2.73 μg g_{cat}^{-1} h^{-1}). Such high performance of the Au/MIL towards NRR could be attributed to the absorption-couple-plasmonic effect between the Au NPs and MIL-100(Cr). This work might provide new strategy for developing an efficient plasmonic photocatalyst to increase photocatalytic NRR performance under visible light at ambient conditions.

Declaration of competing interest

The authors declare that they have no known competing financial interests or personal relationships that could have appeared to influence the work reported in this paper.

Acknowledgments

This work was supported by the National Natural Science Foundation of China (Nos. 21876112, 21876113, 21261140333, 22022608 and 92034301), Shanghai Pujiang Program (No. 20PJ1411800), the National Key Research and Development Program of China (No. 2020YFA0211004), "111" Innovation and Talent Recruitment Base on Photochemical and Energy Materials (No. D18020), Ministry of Education, and Shanghai Key Laboratory of Rare Earth Functional Materials, Shanghai Engineering Research Center of Green Energy Chemical Engineering (No. 18DZ2254200) and Shanghai government (Nos. 18SG41, 309-AC9103-21-413002).

Supplementary materials

Supplementary material associated with this article can be found, in the online version, at doi:10.1016/j.cclet.2022.01.076.

References

[1] H.P. Jia, E.A. Quadrelli, Chem. Soc. Rev. 43 (2014) 547–564.
[2] V. Rosca, M. Duca, M.T. de Groot, M.T.M. Koper, Chem. Rev. 109 (2009) 2209–2244.
[3] N. Zhang, A. Jalil, D. Wu, et al., J. Am. Chem. Soc. 140 (2018) 9434–9443.
[4] N. Gruber, J.N. Galloway, Nature 451 (2008) 293–296.
[5] R.D. Milton, R. Cai, S. Abdellaoui, et al., Angew. Chem. Int. Ed. 56 (2017) 2680–2683.
[6] V. Fourmond, C. Léger, Angew. Chem. Int. Ed. 56 (2017) 4388–4390.
[7] K. Honkala, A. Hellman, I.N. Remediakis, et al., Science 307 (2005) 555–558.
[8] S. Licht, B. Cui, B. Wang, et al., Science 345 (2014) 637–640.
[9] C.J.M. van der Ham, M.T.M. Koper, D.G.H. Hetterscheid, Chem. Soc. Rev. 43 (2014) 5183–5191.
[10] Y. Liu, Q. Li, X. Guo, et al., Adv. Mater. 32 (2020) 1907690.

[11] X. Wang, S. Qiu, J. Feng, et al., Adv. Mater. 32 (2020) 2004382.
[12] J. Di, J. Xia, M.F. Chisholm, et al., Adv. Mater. 31 (2019) 1807576.
[13] C. Ling, X. Niu, Q. Li, A. Du, J. Wang, J. Am. Chem. Soc. 140 (2018) 14161–14168.
[14] H. Zhao, W. Wang, H. Zhang, et al., Angew. Chem. Int. Ed. 58 (2019) 16644–16650.
[15] J. Yuan, X. Yi, Y. Tang, et al., Adv. Funct. Mater. 30 (2020) 1906983.
[16] T. Hou, H. Peng, Y. Xin, et al., ACS Catal. 10 (2020) 5502–5510.
[17] Z. Zhao, C. Choi, S. Hong, et al., Nano Energy 78 (2020) 105368.
[18] J. Schneider, M. Matsuoka, M. Takeuchi, et al., Chem. Rev. 114 (2014) 9919–9986.
[19] M. Kapilashrami, Y. Zhang, Y.S. Liu, A. Hagfeldt, J. Guo, Chem. Rev. 114 (2014) 9662–9707.
[20] H. Hirakawa, M. Hashimoto, Y. Shiraishi, T. Hirai, J. Am. Chem. Soc. 139 (2017) 10929–10936.
[21] J. Yang, Y. Guo, R. Jiang, et al., J. Am. Chem. Soc. 140 (2018) 8497–8508.
[22] Y. Zhao, Y. Zhao, R. Shi, et al., Adv. Mater. 31 (2019) 1806482.
[23] G. Dong, W. Ho, C. Wang, J. Mater. Chem. A 3 (2015) 23435–23441.
[24] R. Guan, D. Wang, Y. Zhang, et al., Appl. Catal. B: Environ. 282 (2021) 119580.
[25] G. Song, R. Gao, Z. Zhao, et al., Appl. Catal. B: Environ. 301 (2022) 120809.
[26] I. Thomann, B.A. Pinaud, Z. Chen, et al., Nano Lett. 11 (2011) 3440–3446.
[27] J.H. Wang, M. Chen, Z.J. Luo, et al., J. Phy. Chem. C 120 (2016) 14805–14812.
[28] J. Yang, H. Bai, Y. Guo, et al., Angew. Chem. Int. Ed. 60 (2021) 927–936.
[29] S.Y. Jeong, H.M. Shin, Y.R. Jo, et al., J. Phy. Chem. C 122 (2018) 7088–7093.
[30] R. Shi, Y. Cao, Y. Bao, et al., Adv. Mater. 29 (2017) 1700803.
[31] L. Zhang, N. Ding, L. Lou, et al., Adv. Funct. Mater. 29 (2019) 1806774.
[32] Y. Kim, E.B. Creel, E.R. Corson, et al., Adv. Energy Mater. 8 (2018) 1800363.
[33] S. Wang, L. Chen, X. Zhao, et al., Appl. Catal. B: Environ. 278 (2020) 119312.
[34] W. Zhang, S. Wang, S.A. Yang, X.H. Xia, Y.G. Zhou, Nanoscale 12 (2020) 17290–17297.
[35] H. Reddy, K. Wang, Z. Kudyshev, et al., Science 369 (2020) 423–426.
[36] N. Ortiz, B. Zoellner, S.J. Hong, et al., ACS Appl. Mater. Inter. 9 (2017) 25962–25969.
[37] B.L. Li, H.L. Zou, J.K. Tian, et al., Nano Energy 60 (2019) 689–700.
[38] J. Yang, Y. Guo, W. Lu, R. Jiang, J. Wang, Adv. Mater. 30 (2018) 1802227.
[39] C. Xiao, H. Hu, X. Zhang, ACS Sustain, Chem. Eng. 5 (2017) 10858–10863.
[40] X.L. Yan, S.N. Li, Y.C. Jiang, M.C. Hu, Q.G. Zhai, Inorg. Chem. Commun. 62 (2015) 107–110.
[41] B. Arstad, H. Fjellvåg, K.O. Kongshaug, O. Swang, R. Blom, Adsorption 14 (2008) 755–762.
[42] G.D. Pirngruber, L. Hamon, S. Bourrelly, et al., ChemSusChem 5 (2012) 762–776.
[43] Z. Hu, S. Faucher, Y. Zhuo, et al., Chem. Eur. J. 21 (2015) 17246–17255.
[44] Z. Sumer, S. Keskin, Ind. Eng. Chem. Res. 56 (2017) 8713–8722.
[45] Z. Zhang, Z.Z. Yao, S. Xiang, B. Chen, Energy Environ. Sci. 7 (2014) 2868–2899.
[46] X.L. Hu, F.H. Liu, H.N. Wang, et al., J. Mater. Chem. A 2 (2014) 14827–14834.
[47] L. Li, C. Tang, B. Xia, et al., ACS Catal. 9 (2019) 2902–2908.
[48] L. Han, X. Liu, J. Chen, et al., Angew. Chem. Int. Ed. 58 (2019) 2321–2325.
[49] L. Zhang, X. Ji, X. Ren, et al., Adv. Mater. 30 (2018) 1800191.
[50] J. Chen, H. Wang, Z. Wang, et al., ACS Catal. 9 (2019) 5302–5307.
[51] Y. Wang, M.M. Shi, D. Bao, et al., Angew. Chem. Int. Ed. 131 (2019) 9564–9569.
[52] L. Li, J. Yang, J. Li, et al., Micropor. Mesopor. Mater. 198 (2014) 236–246.
[53] S. Liu, Y. Zhang, Y. Han, et al., Organometallics 36 (2017) 632–638.
[54] J.W. Yoon, H. Chang, S.J. Lee, et al., Nat. Mater. 16 (2016) 526–531.
[55] C.P. Cabello, G. Berlier, G. Magnacca, P. Rumori, G.T. Palomino, CrystEngComm 17 (2015) 430–437.
[56] J. Dong, B. Liu, B. Yang, J. Mol. Struct. 1116 (2016) 311–316.
[57] M. Nazemi, M.A. El-Sayed, Nano Energy 63 (2019) 103886.
[58] G. Li, F. Li, J. Liu, C. Fan, J. Solid State Chem. 285 (2020) 121245.
[59] D.B. Horn, C.R. Squire, Clin. Chim. Acta 14 (1966) 185–194.
[60] C. Hu, X. Chen, J. Jin, et al., J. Am. Chem. Soc. 141 (2019) 7807–7814.
[61] J. Zhang, X. Chen, K. Takanabe, et al., Angew. Chem. Int. Ed. 49 (2010) 441–444.
[62] W. Li, D. Li, W. Zhang, et al., J. Phy. Chem. C 114 (2010) 2154–2159.
[63] H. Jia, A. Du, H. Zhang, et al., J. Am. Chem. Soc. 141 (2019) 5083–5086.